# Weakly bound $^{87}Rb_2$ $(5s_{1/2} + 5p_{1/2})1_g$ molecules: Hyperfine interaction and LeRoy-Bernstein analysis including linear and nonlinear terms

Haikel Jelassi[1,2] and Laurence Pruvost[3]

[1]*National Centre of Nuclear Sciences and Technologies, Technopole Sidi Thabet, 2020 Tunisia*

[2]*Unité de Recherche "Maîtrise et développement des techniques nucléaires à caractère pacifique," Groupe Radiotraitement*

[3]*Laboratoire Aimé Cotton, CNRS II, Université Paris-Sud, ENS-Cachan, F-91405 Orsay, France*

(Received 8 January 2013; revised manuscript received 9 January 2014; published 20 March 2014)

Data on the $(5s_{1/2} + 5p_{1/2})1_g$ $^{87}Rb_2$ state under the $D_1$ limit, provided by a photoassociation experiment on cold atoms, have been analyzed by an improved LeRoy-Bernstein (LRB) approach including linear and nonlinear terms and provide a $c_6$ value of the potential. To do that, using a model for hyperfine structure shifts, we have first subtracted the hyperfine effects in the split lines and deduced the vibrational energies. Then, we have compared three LRB-type models to fit the data. We conclude that the second-order improved LRB is well suited and allows us to deduce an experimental value of $c_6$ [$c_6 = (15.14 \pm 0.05) \times 10^4$ a.u.].

DOI: 10.1103/PhysRevA.89.032514 PACS number(s): 33.20.Tp, 34.50.Rk, 33.15.Pw

## I. INTRODUCTION

In the context of cold-molecule formation when starting from cooled atoms, the photoassociation process is very often the first step of the excitation-deexcitation scheme [1,2]. For that reason, cold-atom photoassociation spectroscopy (PA) is studied even today because it provides accurate and useful data which could determine or predict new routes in cold-molecule formation.

The benefit of photoassociation of cold atoms as a first step relies on the possibility to bind two cold atoms using a laser light and to produce an excited molecule in a bound level [3]. With this process we change the nature of the initial free wave function (two atoms) to a bound-level wave function. Then the produced excited molecule, often a weakly bound one, decays with a reasonable Franck-Condon factor to a ground-state vibrational level. The knowledge of the excited molecule formed in this intermediate state is thus one of the keys of the cold-molecule research field.

In this context cold-atom PA provides accurate data [4–8]. Because the initial two atoms are cold (typically in the 100 mK range) and the laser bandwidth is small enough (typically in the megahertz range), PA is energetically selective, and the excited molecule produced is in a well-defined vibrational level. In addition, because the atoms are initially far from each other, PA produces mainly molecules in very excited levels (long-range molecules). PA therefore constitutes a fruitful method to provide high-resolution data on long-range molecular states.

Consequently, the knowledge of the molecular levels is correlated to the data analysis methods and to the molecular model used to compare the measurements and the values deduced from the models. Many approaches exist, from semianalytical to all-numerical ones and even both combined.

In the process of cold-atom photoassociation, the molecules formed are weakly bound molecules whose binding energy is governed by the long-range interaction. The molecular potential in this region, close to the dissociation limit, is given by its asymptotic form, namely, the dipole-dipole interaction. For homonuclear molecules, depending on the molecular state symmetry, the asymptotic potential is $-1/R^3$ or $-1/R^6$, where $R$ is the internuclear distance.

Such potential forms, with an $R$ power-law dependence, are known to have simple properties, such as an associated binding energy which varies as a power law of the quantum number of the level (here the vibrational quantum number). For molecular levels this property is known as the LeRoy-Bernstein (LRB) formula [9,10]. Nevertheless, the LRB approach is surely incomplete because it does not include any short-range potential effects, neither couplings between molecular potentials nor other interactions such as the hyperfine interaction. It has been shown that the LRB formula improved by additional terms [11,12] or coupled to a quantum defect approach becomes powerful for quantifying short-range effects [12] or detecting couplings [13,14].

In the case of the presence of hyperfine interaction the situation is more complicated. Close to the dissociation limit ($S + P$, for example), only the levels with $\Omega = 0$ ($0_g^-$ or $0_u^+$ in Hund's case (c), for example) have no hyperfine structure. This is true in the first-order approximation. For $\Omega > 0$ the hyperfine splitting exists in the first-order calculation. Depending on the competition between rotation and hyperfine coupling, the structure is strongly mixed or not. The analysis in the strongly mixed case requires accurate determinations of the potentials in the adequate molecular basis. Examples for this situation can be found in $Li_2$ [15–17], $Na_2$ [6,18–20], $K_2$ [21], and $Rb_2$ [5,22,23].

Nevertheless, in the asymptotic range, like in the situation presented in this paper, where the hyperfine interaction is smaller than the binding energy, the hyperfine structure can be evaluated (in an atomlike basis) and subtracted from the data in order to get a system which can be analyzed by a LRB-type method. That is the approach we developed here.

In this paper, we report on the analysis of spectroscopic data of weakly bound levels of the $1_g$ state of $^{87}Rb_2$ converging to the $5s_{1/2} + 5p_{1/2}$ dissociation limit. The data show split line effects due to the hyperfine interaction. We recorded about 60 vibrational levels over a 20 $cm^{-1}$ range below the dissociation limit, and we observed a well-resolved hyperfine structure for many of them. For binding energies less than 5 $cm^{-1}$, we observed a hyperfine splitting into seven components (denoted by $N = -3, -2, -1, 0, 1, 2, 3$). We interpreted the observed number of components by introducing an intermediate basis

 

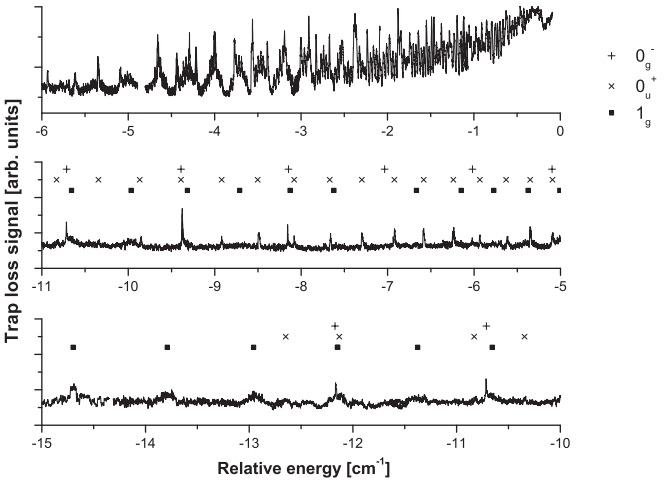


FIG. 1. PA spectrum below the $(5s_{1/2} + 5p_{1/2})$ dissociation limit showing $0_u^+$ (crosses), $0_g^-$ (pluses), and $1_g$ (squares) series. The relative energy is defined relative to the atomic transition $^{87}$Rb $(5S_{1/2}, F = 2) \rightarrow$ $^{87}$Rb $(5P_{1/2}, F' = 2)$ at 12 578.876 cm$^{-1}$.

defined by the nuclear properties and the $1_g$ basis. In this basis, the calculated splitting in a perturbative approach is in good agreement with the measured splitting.

Then, the hyperfine shift of each $N$ component has been subtracted from the energy lines, and the binding energy of each vibrational level is deduced. This procedure increases the set of 60 levels to 120 and therefore allows us to improve the analysis further.

The binding energy data are analyzed using the asymptotic molecular potential (first term, $-1/R^3$, in the dipole-dipole interaction) and the associated LRB formula. We show that the improved LRB formula has to be used to correctly fit the data. Then, we discuss the use of the improved LRB formula including a linear term of energy. Finally, we apply the second-order improved LRB formula up to the second order [24] to analyze the data and to determine the role of the second-order term in the development of the dipole-dipole interaction [in the case of $V(R) = -c_3/R^3 - c_6/R^6$]. We demonstrate, using a residual fit, that the second-order improved LRB $v_D - v = (\epsilon/E_3)^{1/6} + \gamma_1\epsilon + \gamma_{7/6}\epsilon^{7/6} + \gamma_2\epsilon^2$ including three additional high-order terms ($\epsilon$,$\epsilon^{7/6}$, and $\epsilon^2$) is more appropriate for analyzing photoassociation $1g$ state data [24]. Fitting allows us to determine an experimental value of $c_6 = (15.14 \pm 0.05) \times 10^4$ a.u.

## II. EXPERIMENT AND RESULTS

### A. Trap-loss spectroscopy

The experiment consists of photoassociating cold rubidium atoms provided by a magneto-optical trap (MOT) with a laser tuned close to and below the $5s_{1/2} \rightarrow 5p_{1/2}$ atomic transition. As the frequency of the photoassociation laser (PA laser) is resonant with a molecular level of $Rb_2$ (a level of a molecular curve converging to the $5s_{1/2} + 5p_{1/2}$ dissociation limit), an efficient formation of molecules happens, and as a consequence, an atom loss is observed. The PA spectrum is obtained by recording the trap-loss signal while the PA laser is scanned [10]. Such a PA spectrum is shown in Fig. 1.

Details about the experimental setup have been given in previous studies [25,26]. Our MOT operates in a stainless chamber vapor cell where the background pressure is kept in the $10^{-9}$ mbar range by an ionic pump. All the lasers used to prepare the MOT are provided by laser diodes emitting about 50 mW of laser power each at 780-nm wavelength. The trapping laser is provided by a Sanyo diode, with a linewidth of about 1 MHz and tuned 12 MHz to the red of the atomic $5S_{1/2}(F = 2) \rightarrow 5P_{3/2}(F' = 3)$ $^{87}$Rb transition. The repumping laser is generated by a Hitachi diode laser which is locked to the rubidium line $5S_{1/2}(F = 1) \rightarrow 5P_{3/2}(F' = 2)$. The lasers (trapping and repumping) are frequency locked to atomic lines using saturated absorption spectroscopy in Rb vapor glass cells. The detuning of the trapping laser is adjusted via an acoustomodulator. Its total power in the MOT region is about 40 mW ($2 \times 20$ mW because of retroreflected beams), and the beams have Gaussian profiles with $\sim$8-mm waists. The applied quadrupolar magnetic gradient in the MOT region is 14 G/cm. It is generated by two coils in an anti-Helmholz configuration. With these parameters, the produced Rb cold cloud contains about $10^7$ atoms. The radius of the cloud is 0.5 mm, and its temperature is 30 $\mu$K. The atomic density reaches $n \sim 10^{11}$ atoms/cm$^3$.

To photoassociate atoms, a PA laser provided by a widely tunable titanium-sapphire laser (Coherent MBR 110) is superimposed on the Rb sample. The beam power is about 900 mW, and its linewidth is about 1 MHz. At the MOT location, the PA laser beam has a waist of 1 mm, so that its intensity is about 25 KW/cm$^2$. The PA laser promotes colliding pairs of Rb atoms into a specific excited bound level of $Rb_2$. To obtain a spectrum of these molecular levels, we scan the PA laser wavelength and simultaneously record the atomic cloud fluorescence, which gives the cloud atom number and thus the trap loss. The atomic cloud fluorescence is collected onto a photodiode, and the resulting signal is amplified to reach the volt range and to be stored in a computer. The PA laser wavelength is measured with a wavemeter (Burleigh WA 1000) with an accuracy of 300 MHz while the laser is being scanned. A General Purpose Interface Bus connection between the wavemeter and the computer ensured data storage. Typically, each scan of the PA laser covers 1 cm$^{-1}$ ($\sim$30 GHz) and takes 600 s and is recorded with typically 3000 data points (each 0.2 s). For each scan, we have checked the linearity of the frequency scan versus time and have used it to improve the resolution of the wavelength measurement by a factor 10 (at least). So accuracy is better than 0.002 cm$^{-1}$; we take this value in the following. With a succession of scans we obtain the spectrum over 20 cm$^{-1}$ (see Fig. 1).

The PA laser wavelength is chosen to be red detuned from the $D_1$ atomic line at 795 nm in order to explore the molecular states near the $5s_{1/2} + 5p_{1/2}$ limit. The obtained spectra were calibrated relative to the atomic transition $^{87}$Rb $(5S_{1/2}, F = 2) \rightarrow$ $^{87}$Rb$(5P_{1/2}, F' = 2)$, whose energy is 12 578.876 cm$^{-1}$. In the scanned region (about 20 cm$^{-1}$ of PA laser detuning) the losses reach about 30%. Beyond that, the photoassociation process is less efficient, and it is very difficult to detect a trap loss.

### B. Observation of a hyperfine splitting in the $(5s_{1/2} + 5p_{1/2})1_g$ levels

The PA spectrum below the $(5s_{1/2} + 5p_{1/2})$ dissociation limit is shown in Fig. 1. In this spectrum, we identified three

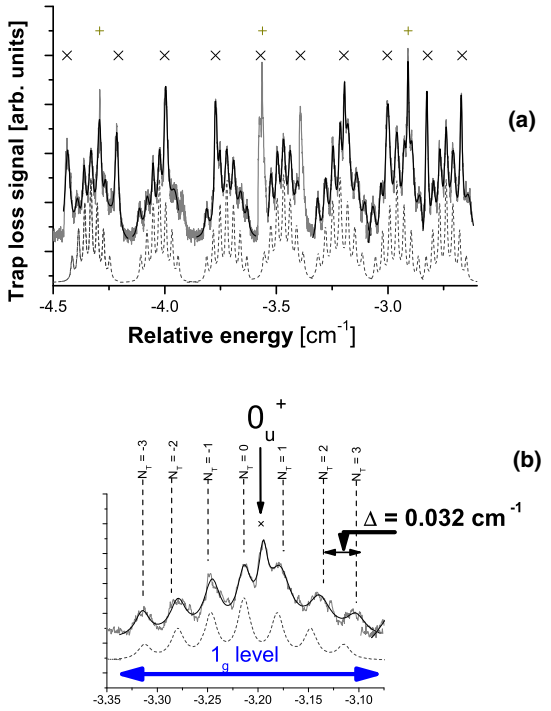


FIG. 2. (Color online) Hyperfine structure in $1_g$ resonances: (a) seven resonances with resolved hyperfine components. (b) Close-up of the resonance around 3.21 cm$^{-1}$. Gray lines: experimental spectrum ($0_u^+$ and $0_g^-$ levels are marked by crosses and pluses, respectively). Black lines: fitting spectrum with a multi-Lorentzian function to determine the resonances energies. Dashed dark gray lines: theoretical curve of seven weighted Lorentzian profiles separated by $\Delta = 0.032$ cm$^{-1}$ with the weights equal to the degeneracies, namely, $4 - |N_T|$.

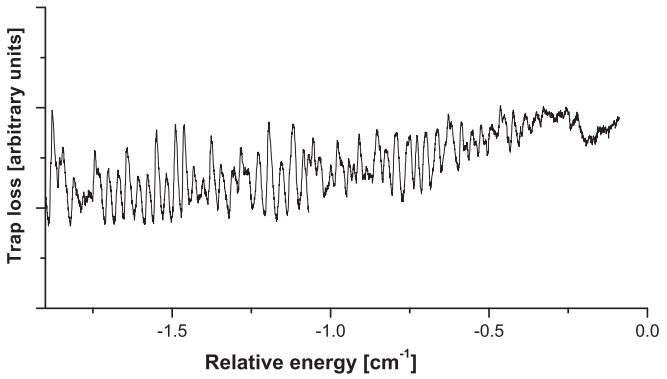


FIG. 3. PA spectrum below $(5s_{1/2} + 5p_{1/2})$ dissociation limit for PA detuning less than 1.8 cm$^{-1}$: the $0_g^-$, $0_u^+$, and $1_g$ resonances are not clearly identified.

vibrational series corresponding to the $1_g$, $0_u^+$, and $0_g^-$ attractive molecular states. The observed levels of the $0_u^+$ and $0_g^-$ states have been studied and analyzed in previous works [12,13]. For these series, an analysis based on the vibrational quantum defect allowed us to quantify the short-range potential effects in the case of the $0_g^-$ state [12] and a coupling with a neighboring series via the spin-orbit interaction in the case of the $0_u^+$ state [13].

In this paper, we focus on the $1_g$ molecular state. For a PA laser detuning larger than 5 cm$^{-1}$, the $1_g$ resonances are broad (Fig. 1). The width of the resonances is about 0.12 cm$^{-1}$.

In the [1.8 cm$^{-1}$, 5 cm$^{-1}$] range, the $1_g$ resonances are split into seven clearly resolved components [see the close-up in Fig. 2(a)]. The splitting origin is the hyperfine interaction in the molecule. The seven components are denoted by $N_T$, where $N_T$ varies from $-3$ to 3 [Fig. 2(b)] and is spaced by $\sim$0.03 cm$^{-1}$. We will explain in the following this notation and this splitting value.

For a PA laser detuning less than 1.8 cm$^{-1}$, it is quite difficult to clearly identify $0_g^-$, $0_u^+$, and $1_g$ resonances, as is shown in Fig. 3. For that reason we limited our analysis to the [1.8 cm$^{-1}$, 21 cm$^{-1}$] energy range.

The energies of the $1_g$ resonances and of the components that we have observed are listed in Tables IV and V in Appendix A. The spectrum analysis consists of measuring the energy of each resonance and each component by using a local fitting with a Lorentzian shape. The measured binding energy $\varepsilon$ is given relative to the atomic transition $^{87}$Rb $(5S_{1/2}, F = 2) \rightarrow {}^{87}$Rb $(5P_{1/2})$ at 12 578.780 cm$^{-1}$. The data are presented in two tables. Table IV lists binding energies of broad $^{87}$Rb $(5s_{1/2} + 5p_{1/2})1g$ resonances. In that case we give the center of the resonance as the binding energy. Table IV also gives the relative vibrational quantum number, i.e., $v_D - [v]$. Table V lists the binding energies of the components for the 12 observed split resonances. For three of them, it was not possible to clearly assign the binding energy of the seven $N_T$ components.

## III. THE $1_g$ STATE DESCRIPTION INCLUDING THE HYPERFINE INTERACTION

### A. Generalities

Early groups working on PA spectroscopy of cold atoms pointed out the role of the hyperfine interaction in long-range excited molecules. They pointed out that the binding energy of the molecule or the rotational energy is small and thus on the same order of magnitude as the hyperfine interaction. In this case, mixing of potential curves appears, and a description with an adapted basis is required. This problem was well illustrated in Ref. [27], where the calculated PA spectrum of $Na_2$ for the $v = 80$ vibrational level shows that the hyperfine and rotational structures are on the same order of magnitude (see Fig. 3 of Ref. [27]). Williams and Julienne [27] showed that the correct basis to describe the molecule is $F = J + I$, obtained by coupling the molecular number $J$ with the total nuclear spin $I = I_1 + I_2$ ($I_1$ and $I_2$ being the atomic nuclear spins). For a dimer, the good quantum number is the projection of $F$ along the molecular axis. This description gives many molecular states and thus many molecular curves (see, for example, Fig. 2 of Ref. [27]).

Using this multitude of curves to compare the experimental results and the molecular description is not easy. The numerous potential curves in the asymptotic region are remarkably grouped by packets, in which the curves are nearly parallel. That means that the molecular curves are only energy shifted relative to each other. At large interatomic distances the curves are energy shifted relative to the molecular curve obtained in the usual basis of Hund's case (c). For the $^{87}Rb_2$ molecule, the

TABLE I. The $c_3$ and $c_6$ expressions and values for the $(5s_{1/2} + 5p_{1/2})1_g$ state. As detailed in [12], we take $C_3 = 8.949(10)$ a.u., $A = 158.39893662\ \text{cm}^{-1} \equiv 7.2171865892 \times 10^{-4}$ au, $C_6^{\Pi} = 8.05 \times 10^3$ a.u., and $C_6^{\Sigma} = 12.91 \times 10^3$ a.u. Thus $\frac{28}{27}C_3^2/A = 11.5073 \times 10^4$ a.u., and $(2C_6^{\Pi} + C_6^{\Sigma})/3 = 0.967 \times 10^4$ a.u.

| Expression | Value |
|---|---|
| $c_3 = \frac{2}{3}C_3$ | 5.966 a.u. [29] |
| $c_6 = \frac{2C_6^{\Pi}+C_6^{\Sigma}}{3} + \frac{28C_3^2}{27A}$ | 12.4743 $10^4$ a.u. [30] |
| $\epsilon_{\text{scale}} = c_3^2/c_6$ | 62.6 $\text{cm}^{-1}$ |

hyperfine potential-energy curves are illustrated by Fig. 6 of Ref. [22].

These observations lead us to describe the molecule in the basis of Hund's case (c) first and then to add the hyperfine interaction via an intermediate basis.

### B. The $1_g$ molecular potential in Hund's case (c)

Close to the dissociation limit, in the energy range studied in this paper, the spin-orbit interaction is large compared to the binding energy of the vibrational level, so the dimer is described in the basis of Hund's case (c) [28]. In this basis, at a large value of the internuclear distance $R$, the $1_g$ molecular potential is given by the dipole-dipole interaction, and its development, including the first two terms, is

$$V(R) = -c_3/R^3 - c_6/R^6, \tag{1}$$

where $c_3$ and $c_6$ are effective coefficients related to atomic matrix elements. Table I gives the $c_3$ and $c_6$ expressions and the values for the $Rb_2$ $(5s_{1/2} + 5p_{1/2})1_g$ state.

### C. Vibrational energy: LeRoy-Bernstein approach

The vibrational energies (binding energies) are the eigensolutions of the Schrödinger equation for the molecular potential given by Eq. (1). In the context of weak binding energies the solutions can be found using the Wentzel-Kramers-Brillouin (WKB) approximation and the Bohr-Sommerfeld quantization.

If the potential given by Eq. (1) is limited to its first term, namely, $-c_3/R^3$, the WKB solution is the well-known LRB formula [9]. The LRB formula gives the eigenenergies of the Schrödinger equation in the case of an attractive potential $-c_n/R^n$, with $n \neq 2$ [9]. For $n = 3$, the binding energy $\epsilon_v$ of the vibrational level labeled $v$ is given by

$$\epsilon_v = E_3(v_D - v)^6, \tag{2}$$

where $v_D$ is a noninteger number and $E_3$ is an energy constant related to $c_3$ and the reduced mass $\mu$. According to the LRB notations, $E_3 = H_3^6$, where $H_3$ is a quantity defined by $H_3^{-1} = \frac{\sqrt{2\mu}}{\sqrt{\pi}}\frac{c_3^{1/3}}{\hbar}\frac{\Gamma(5/6)}{\Gamma(4/3)}$, with $\Gamma$ being the Euler gamma function. With the values of Table I, we find $E_3 = 11.786 \times 10^{-12}\ \text{cm}^{-1}$. We denote it as $E_3^0$.

Usually, data analysis done using the LRB formula (2) is performed by plotting the quantity $n = \text{integer}[v_D] - v$ versus the measured binding energy $\epsilon$ and then by fitting the obtained curve by the function $a + [(\epsilon - \epsilon_0)/E_3]^{1/6}$. The fitting procedure provides $a$, $\epsilon_0$, and $E_3$ (see Ref. [7], for example). The parameter $a$ gives the noninteger part of $v_D$. The parameter $\epsilon_0$ allows us to adjust slightly the value of the dissociation limit, and the energy constant $E_3$ allows the determination of $c_3$.

The LRB formula is applicable when the term $-c_6/R^6$ in formula (1) is negligible compared to $-c_3/R^3$. This condition expressed on the energy variable gives a binding energy $\epsilon_v$ which has to be less than $\epsilon_{\text{scale}} = c_3^2/c_6$ [24]. For $Rb_2$ in the $1_g$ state, with the values of Table I, one gets $\epsilon_{\text{scale}} \sim 60\ \text{cm}^{-1}$. With the data considered in this paper we have $\epsilon < 20\ \text{cm}^{-1}$; thus the condition $\epsilon \ll \epsilon_{\text{scale}}$ is not fulfilled.

The fitting method using the LRB formula is quite powerful; nevertheless, for very accurate studies, it has been shown that the LRB formula has to be corrected in order to include short-range potential effects and terms in the potential multipolar expansion. It has been shown that the main additional term to the LRB formula is linear [11,12], giving the improved LRB formula:

$$v_D - v = (\epsilon_v/E_3)^{1/6} + \gamma\epsilon_v, \tag{3}$$

where $\gamma$ is a parameter connected to the short-range potential. In Ref. [12] it was shown that the parameter $\gamma$ is connected to short-range characteristics of the potential, e.g., the repulsive region of the molecular potential.

In a more accurate approach [24], a model including the $-c_6/R^6$ term and the short-range potential has shown that the LRB formula has to be modified with three additional terms: one is linear as a function of the energy, another depends on $\epsilon_v^{7/6}$, and the last one is quadratic as a function of the energy. Because this approach includes the second-order term in the multipolar development of the molecular potential, the corresponding improved LRB formula, called the second-order improved LRB formula, is

$$v_D - v = (\epsilon_v/E_3)^{1/6} + \gamma_1\epsilon_v + \gamma_{7/6}\epsilon_v^{7/6} + \gamma_2\epsilon_v^2. \tag{4}$$

In this second improved LRB formula $\gamma_1$, $\gamma_{7/6}$, and $\gamma_2$ depend on the short-range potential and on the quantity $c_3^2/c_6$ (see details in Refs. [12,24]).

### D. Hyperfine structure in the $1_g$ state

The Hund (c) basis takes into account only the spin-orbit effect in the atoms. For a complete description of the molecule, the hyperfine interaction must be included. Its order of magnitude is, in a crude approach, given by the atomic hyperfine interaction in the $5s_{1/2}$ and $5p_{1/2}$ atomic levels. The atomic hyperfine splitting in the atomic ground state $5s_{1/2}$, namely, the $F = 1 - F = 2$ separation, is $\Delta^{hf}_{5s_{1/2}} = 6.834\ \text{GHz}$. In the $5p_{1/2}$ excited state it is $\Delta^{hf}_{5p_{1/2}} = 0.816\ \text{GHz}$. These values define a limit for the validity of the long-range potential form given by Eq. (1). Typically, for a binding energy that is very large compared to $\Delta^{hf}_{5s_{1/2}} + \Delta^{hf}_{5p_{1/2}} \sim 0.25\ \text{cm}^{-1}$, the hyperfine effects can be added in a perturbative approach.

To apply the perturbative approach we define an intermediate basis denoted $|1_g M = \pm 1\rangle|I_1 N_1\rangle|I_2 N_2\rangle$, where $I_1 = I_2 = 3/2$ is the $^{87}$Rb nuclear spin and $N_1$ and $N_2$ are the associated projections. Details about the basis and the calculation of the energy shift are given in Appendix B.

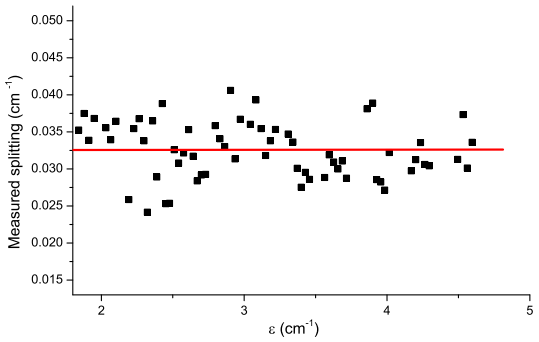


FIG. 4. (Color online) Measured hyperfine energy splittings in the $1_g$ resonances (those with seven resolved components). The red line is the mean value of 63 measured hyperfine energy splitting values.

The intermediate basis is convenient to perform the calculation (because many matrix elements are zero), and in a perturbative approach the energy correction only depends on $N_T = N_1 + N_2$. The energy correction due to the hyperfine interaction is

$$\Delta_{hf}(N_T) = \Delta N_T, \tag{5}$$

with $\Delta = \frac{1}{8}(\Delta^{hf}_{5s_{1/2}} + \Delta^{hf}_{5p_{1/2}}) = 0.956$ GHz $= 0.032$ cm$^{-1}$.

The allowed values of $N_1$ and $N_2$ provide seven values of $N_T$ in the range $[-3,3]$. Each level degeneracy is $4 - |N_T|$.

The splitting of the $1_g$ resonances into seven components has been observed for binding energies ranging from 1.8 to 5 cm$^{-1}$ (Fig. 2 and Table V), i.e., 12 resonances. For eight of them, the seven components are clearly resolved and identified. From the measured energy position of the components, we have deduced the hyperfine energy splittings and plotted them in Fig. 4. The statistics on the 63 values gives $0.0325\pm 0.0038$ cm$^{-1}$, which is in good agreement with the expected value, i.e., $\Delta = 0.032$ cm$^{-1}$.

The degeneracies, measured by the peak amplitudes, are also well described by this model [see Fig. 2(b)], except when a $0^-_g$ or a $0^+_u$ resonance overlaps the $1_g$ resonances. Notice that the red (dark gray) line in Fig. 2(b), which represents a theoretical model with seven Lorentzian functions weighted by the degeneracies and spaced by a value of $\Delta$, is not a fitting curve and is quite in agreement with the experimental spectrum.

### E. Total energy

The total binding energy of a $1_g$ component (level including the hyperfine interaction), which is a positive quantity defined by the energy at the dissociation limit minus the level energy and denoted $\epsilon_T$, is then

$$\epsilon_T = \epsilon_v - \Delta_{hf}(N_T), \tag{6}$$

where $\epsilon_v$ is the vibrational binding energy associated with the potential $V(R)$.

For each level, because the quantity $\Delta_{hf}(N_T)$ is known, we can deduce the vibrational binding energy $\epsilon_v$ associated with the $1g$ resonance. As a consequence, in the case of a $1_g$ resonance with seven resolved hyperfine components, we get seven measurements of the $1g$ vibrational binding energy. Therefore this increases the number of available experimental data points for the vibrational binding energy $\epsilon_v$ of the $1_g$ state in order to analyze them with LRB or improved LRB approaches. With our set of data we thus extract a set of 126 energy values of $\epsilon_v$.

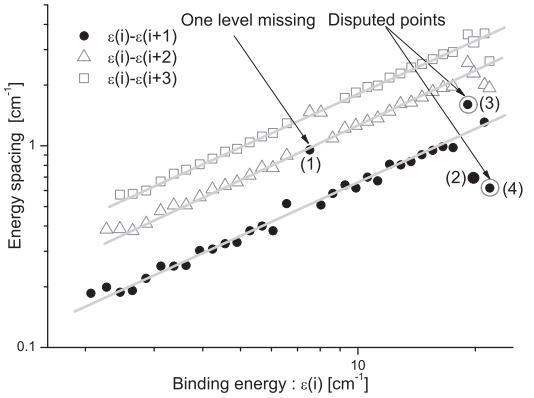


FIG. 5. Energy spacings between the $1_g$ vibrational level and its first neighbor (solid circles) obtained by $\epsilon(i) - \epsilon(i-1)$, its second neighbor (triangles) obtained by $\epsilon(i) - \epsilon(i-2)$, and its third neighbor (squares) obtained by $\epsilon(i) - \epsilon(i-3)$. For each vibrational level, three energy spacings are plotted as a function of $\epsilon(i)$. The index $i$ is an attribute integer value for each line (see Tables IV and V). Number (1) concerns a nondetected resonance. Number (2) concerns the point located at 19.81 cm$^{-1}$. Open circles: two nonregular points (3) at 19.12 and (4) at 21.75 cm$^{-1}$. Gray lines help guide the eye.

## IV. DATA ANALYSIS

### A. Energy progression of the levels

In order to attribute the $v_D - v$ value to the resonances, we checked at the energy progression of the levels. We attribute an integer value denoted $i$ to each resonance (see Tables IV and V). $i$ should be the integer $[v_D] - v$, but because we do not know the exact value of $v_D$, $i$ is defined relatively. For a given $i$, levels $i+1$, $i+2$, and $i+3$ are called, respectively, the first, second, and third neighbors. For each $i$ resonance of Table IV we calculate the quantities $\epsilon(i) - \epsilon(i+1)$, $\epsilon(i) - \epsilon(i+2)$, and $\epsilon(i) - \epsilon(i+3)$ from the mean $\epsilon$ column and plot them versus $\epsilon(i)$ (see Fig. 5). For the lines in Table V we only take the energy values of $N_T = 0$ lines.

As shown in Fig. 5, in log-log scale we observe that the points are aligned. On the lower line, which gives the energy distance to the first neighbor, we observe a hole between 6.5 and 7.5 cm$^{-1}$. The corresponding data point [black point denoted by (1)] is located on the second line, which is the energy distance to the second neighbor. The missing level (or undetected level) numbered $i = 20$ is indicated as a "not detected" level in Table IV.

For points denoted (2), (3), and (4), a fine analysis of the spacing allows us to deduce that one level has not been detected (may not be detectable) and that two others (at 19.12 cm$^{-1}$ and at 21.75 cm$^{-1}$) do not belong to the $1_g$ series. The nondetected level is indicated in Table IV with $i = 5$ as "not detected." As a consequence, for level $i = 3$, at 19.81 cm$^{-1}$, marked by (2) in Fig. 5, $\epsilon(3) - \epsilon(4)$ is out of the first slope, $\epsilon(3) - \epsilon(6)$ is on the second slope, and $\epsilon(3) - \epsilon(7)$ is on the third slope. We thus deduce that $i = 3$, at 19.81 cm$^{-1}$, belongs to the $1_g$ series. The energy spacing analysis allows us to attribute the value of $v_D - v$ to each resonance.

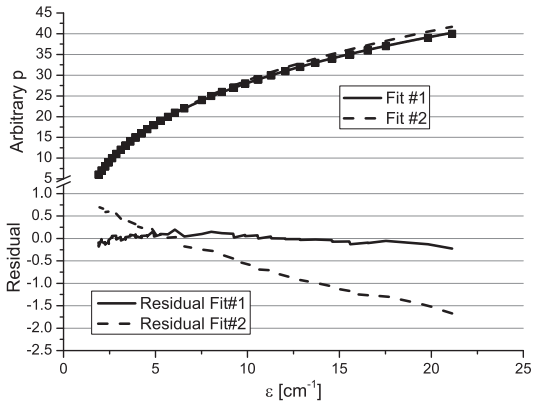


FIG. 6. Analysis of the 125 points using the LRB formula of Eq. (2). The top view shows experimental points and their fit curves. The bottom view presents the residual for each fit. Fit 1, shown by the black line, gives $E_3 = (17.409 \pm 0.07) \times 10^{-12}$ cm$^{-1}$, $y_0 = -63.05 \pm 0.06$, and $\chi^2 = 0.00552$. Fit 2 dashed black lines gives $y_0 = -68.55 \pm 0.06$ and $\chi^2 = 0.44423$; $E_3$ was fixed to be $E_3^0 = 11.786 \times 10^{-12}$ cm$^{-1}$.

### B. Analysis using the LeRoy-Bernstein formula

In a natural approach, the set of 125 labeled ($p$ attributed) levels is analyzed using the LRB formula (2). We have done two fits, fit 1 and fit 2, using the following fitting function: $y = y_0 + (\frac{x}{E_3})^{1/6}$. Fit 1 gives $y_0 = -63.05 \pm 0.06$ and $E_3 = (17.409 \pm 0.07) \times 10^{-12}$ cm$^{-1}$. Even if the corresponding residual curve, shown in Fig. 6, is close to $y = 0$ (from $-0.227$ to $+0.198$), the obtained value of $E_3$ does not correspond to the expected one ($E_3^0 = 11.786 \times 10^{-12}$ cm$^{-1}$). They are different by 48%. Such a difference indicates that the model used is not accurate enough. It suggests that a fitting function including an additional nonlinear term would be more appropriate.

Fit 2 is done using an imposed $E_3 = E_3^0 = 11.786 \times 10^{-12}$ cm$^{-1}$. It gives $y_0 = -68.55 \pm 0.06$. The corresponding fit residue clearly exhibits a nonlinear behavior versus $\epsilon$, indicating that the LRB is not sufficient in such a situation.

Both fits undoubtedly show the need for an improved LRB formula [12]. Such behavior has already been observed in our previous works. In fact, we have demonstrated the role of the linear term in the LRB model.

First, in the case of $^{87}Rb_2$ $(5s_{1/2} + 5p_{1/2})0_g^-$, it has been shown that the additional term is linear [12]. This term is also required in the case of series with perturbations (analysis by the Lu-Fano graph), as shown in the cases of $^{87}Rb_2$ $(5s_{1/2} + 5p_{1/2})0_u^+$ [13], $^{133}Cs_2$ $(6s_{1/2} + 6p_{1/2})0_u^+$ [14], and $^{133}Cs_2$ $(6s_{1/2} + 6p_{1/2})0_g^-$ [31–33].

### C. Analysis using the improved LeRoy-Bernstein formula

In this section, we apply the improved LRB formula [Eq. (3)] and the second-order improved LRB formula [Eq. (4)] in order to examine the effects of the $-c_6/R^6$ term. In the rest of this section, $E_3$ will be taken to be $E_3^0 = 11.786 \times 10^{-12}$ cm$^{-1}$.

Our approach relies on the Ref. [24], where we have shown that parameters are related to the short-range potential (i.e., its barrier) and to the second-order term in the long-range potential, namely, $-c_6/R^6$. Our analysis also showed that in the case of the $1_g$ state of alkalis (Cs, Rb, K) the short-range effect

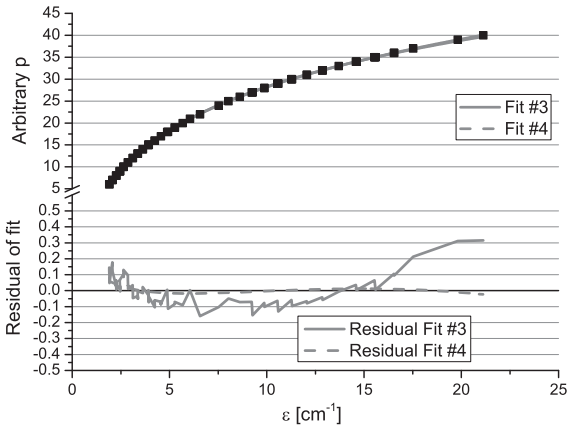


FIG. 7. Analysis of the 125 points using the improved LRB formula of Eq. (3) (fit 3) and using the second-order improved LRB formula of Eq. (4) (fit 4). The top view shows experimental points and their fit curves. The bottom view presents the residual for each fit. For two fits, $E_3$ was set as $E_3^0 = 11.786 \times 10^{-12}$ cm$^{-1}$. Fit 3 (gray line) gives $y_0 = -67.67 \pm 0.01$, $\gamma = -0.135 \pm 0.002$ (cm$^{-1}$)$^{-1}$, and $\chi^2 = 0.0074$. Fit 4 dashed gray line gives $y_0 = -67.511 \pm 0.002$, $\gamma_1 = -0.2223 \pm 0.0004$ (cm$^{-1}$)$^{-1}$, $\epsilon_{\text{scale}} = 51.58 \pm 0.17$ cm$^{-1}$, and $\chi^2 = 0.00019$.

is negligible compared to that of $-c_6/R^6$. In that case $\gamma = \gamma_1$, $\gamma_{7/6}$, and $\gamma_2$ are given by Eqs. (24), (25), and (26) of Ref. [24]. They are only related to $c_3$ and $\epsilon_{\text{scale}}$ by the following formulas:

$$\gamma_1 = \frac{\sqrt{2\mu}}{h} c_3^{1/3} \epsilon_{\text{scale}}^{-5/6} \frac{\Gamma\left(\frac{4}{3}\right)\Gamma\left(-\frac{5}{6}\right)}{3\sqrt{\pi}}, \tag{7}$$

$$\gamma_2 = -\frac{\sqrt{2\mu}}{h} c_3^{1/3} \epsilon_{\text{scale}}^{-5/6} \frac{2}{3\epsilon_{\text{scale}}} \frac{\Gamma\left(\frac{4}{3}\right)\Gamma\left(-\frac{5}{6}\right)}{3\sqrt{\pi}}, \tag{8}$$

$$\gamma_{\frac{7}{6}} = \frac{\sqrt{2\mu}}{h} c_3^{1/3} \frac{\sqrt{\pi}}{3} \frac{\Gamma\left(\frac{5}{6}\right)}{\Gamma\left(\frac{4}{3}\right)} \frac{2}{7\epsilon_{\text{scale}}}. \tag{9}$$

In this framework, we first start by analyzing data using Eq. (3). For that we fit data using the $y = y_0 + (\frac{x}{E_3})^{1/6} + \gamma$ $x$ function, where $E_3$ is equal to $E_3^0$. Fit 3, shown in Fig. 7, gives $y_0 = -67.67 \pm 0.01$ and $\gamma = -0.135 \pm 0.002$(cm$^{-1}$)$^{-1}$ with $\chi^2 = 0.0074$ and a residue curve ranging from $-0.160$ to $+0.316$. According to Eq. (7), we deduce that $\epsilon_{\text{scale}}^{\#3} = 321.763 \pm 4.767$ cm$^{-1}$. This value is quite large compared to the estimated one in Sec. IIIC. This indicates that the improved LRB formula [Eq. (3)] is not accurate enough to match the data.

In an advanced analysis, we use Eq. (4) and the following fitting function: $y = y_0 + (\frac{x}{E_3})^{1/6} + \gamma_1\ x + \gamma_{7/6} x^{7/6} + \gamma_2 x^2$. Because the parameters $\gamma_1, \gamma_{7/6}$, and $\gamma_2$ are correlated, in addition we impose

$$\gamma_{7/6} = -0.19022 \epsilon_{\text{scale}}^{-1/6} \gamma_1 \tag{10}$$

$$\gamma_2 = -\tfrac{2}{3} \epsilon_{\text{scale}}^{-1} \gamma_1 \tag{11}$$

Such a procedure (fit 4 of Fig. 7) provides $y_0 = -67.511 \pm 0.002$, $\gamma_1 = -0.2223 \pm 0.0004$ (cm$^{-1}$)$^{-1}$, $\epsilon_{\text{scale}}^{\#4} = 51.58 \pm 0.17$ cm$^{-1}$, with $\chi^2 = 0.00019$ and a residue curve ranging from $-0.024$ to $+0.061$. Clearly, fit 4 is better than fit 3. $\chi^2$ is reduced by a factor of 40. The residue curves show a better adequation of the second-order improved LRB formula for

large binding energies, confirming the role of the $\epsilon^{7/6}$ and $\epsilon^2$ terms.

### D. Discussion

Fit results and deduced parameters are regrouped in Table II.

The value of $\epsilon_{\rm scale}$ provided by fit 4, namely, $\epsilon^{\#4}_{\rm scale} = 51.58$ cm$^{-1}$, is in good agreement with the estimated one ($\epsilon_{\rm scale} = 62.6$ cm$^{-1}$). They differ from each other by 17.5%, which is not large, relatively speaking, if we take into account the uncertainty on $\epsilon_{\rm scale}$. Indeed, in the expression of $\epsilon_{\rm scale} = c_3^2/c_6$, only $c_3$ is well known, but $c_6$ includes $C_6^\Pi$ and $C_6^\Sigma$, which have never been determined experimentally. The values of $C_6^\Pi$ and $C_6^\Sigma$ have been determined only by theoretical calculations. From our fit procedure we extract $\epsilon_{\rm scale}$, with $\frac{\Delta\epsilon_{\rm scale}}{\epsilon_{\rm scale}} = 0.3\%$; thus $c_6 = (15.14 \pm 0.05) \times 10^4$ a.u. This value differs from the calculated one given in Table I by 21%. It is extracted with $\frac{\Delta c_6}{c_6} = 0.3\%$ also.

From the $c_6$ value, we do not deduce the values of $C_6^\Pi$ and $C_6^\Sigma$, only the combination $\frac{2C_6^\Pi + C_6^\Sigma}{3} = (3.64 \pm 0.05) \times 10^4$ a.u. The value is not very accurate, and it is far (3.65 times higher) from the value given in Table I. The combination is found with $\frac{\Delta\frac{2C_6^\Pi+C_6^\Sigma}{3}}{\frac{2C_6^\Pi+C_6^\Sigma}{3}} = 1.4\%$.

In order to check, we have done another fit (named fit 5 and not plotted in Fig. 7) wherein $E_3$ becomes a fit parameter. The fit result is $y_0 = -66.104 \pm 0.263$, $E_3 = 13.304 \pm 0.315 \times 10^{-12}$ cm$^{-1}$, $\gamma_1 = -0.143 \pm 0.018$ (cm$^{-1}$)$^{-1}$, and $\epsilon^{\#5}_{\rm scale} = (63.86 \pm 8.48)$ cm$^{-1}$. We deduced from $E_3$ and $\epsilon^{\#5}_{\rm scale}$ the multipolar coefficient $1_g$ potential values $c_3 = 5.615 \pm 0.067$ a.u. and $c_6 = c_3^2/\epsilon^{\#5}_{\rm scale} = (10.84 \pm 1.69) \times 10^4$ a.u. The values differ from calculated values given in Table I by 6% and 13%, respectively. We deduce the value of the combination $\frac{2C_6^\Pi + C_6^\Sigma}{3} = (0.65 \pm 0.18) \times 10^4$ a.u., which is 1.53 times smaller than that given in Table I. The combination value is given with $\frac{\Delta\frac{2C_6^\Pi+C_6^\Sigma}{3}}{\frac{2C_6^\Pi+C_6^\Sigma}{3}} = 27.7\%$.

According to Table II, which summarizes the results of all fits, one can consider fit 4 more appropriate than fit 5 even if the results of fit 5 seem better overall. There are several reasons why we believe that fit 4 is more relevant than fit 5:

(i) $\chi^2$ of fit 4 is 7 times smaller than that deduced from fit 5.

(ii) Fit 5 gives a $c_3$ value with a 6% deviation relative to the theoretical value. Then this value presents a very large disagreement on $c_3$ compared to previous works (amply confirmed by several previous works either experimentally or theoretically).

(iii) $\frac{2C_6^\Pi+C_6^\Sigma}{3}$ is given with 1.4% relative accuracy for fit 4, while the relative accuracy reaches 27.7% for fit 5.

In Table III, we report for comparison the quantity $\frac{2C_6^\Pi+C_6^\Sigma}{3}$ extracted from this work and two other works ([34] and [35]). The two others works, a theoretical one and an experimental one, are in good agreement each other. However, our values, extracted from fits 4 and 5, are not in good agreement. We think that this discrepancy occurs for several reasons:

(i) Our fitting model is based on crude approximations. In Ref. [14] we suppose that the potential is $V(R) = -c_3/R^3 - c_6/R^6$, truncated at an internuclear distance called $R_-$.

(ii) In this work, we fitted a limited set of data with binding energies $\epsilon < 20$ cm$^{-1}$. The authors of Ref. [35] used a larger set of vibrational levels (71 levels) belonging to the $0_g^-(P_{3/2})$ pure long-range electronic state of the $^{87}Rb_2$ molecule to determine more accurate $C_6^\Pi$ and $C_6^\Sigma$.

In addition, we propose that the value of $c_6$, which has been determined only twice previously, must be revisited by means of theoretical calculations and/or by additional experiments.

TABLE II. Results of fits: Fit parameters and deduced values of $E_3$, $\epsilon_{\rm scale}$, $c_3$, $c_6$, and $\frac{2C_6^\Pi+C_6^\Sigma}{3}$.

| | Fit 1 | Fit 2 | Fit 3 | Fit 4 | Fit 5 |
|---|---|---|---|---|---|
| Fitting function | $y_0 + (\frac{x}{E_3})^{1/6}$ | $y_0 + (\frac{x}{E_3})^{1/6}$ | $y_0 + (\frac{x}{E_3})^{1/6}$ $+\gamma_1 x$ | $y_0 + (\frac{x}{E_3})^{1/6}$ $+\gamma_1 x$ $-\frac{2}{3}\epsilon_{\rm scale}^{-1}\gamma_1 x^2$ $-0.19022\epsilon_{\rm scale}^{-1/6}\gamma_1 x^{7/6}$ | |
| | | | Fit parameters | | |
| $\chi^2$ | 0.00545 | 0.44087 | 0.0074 | 0.00019 | 0.00133 |
| $y_0$ | $-63.05 \pm 0.06$ | $-68.55 \pm 0.06$ | $-67.67 \pm 0.01$ | $-67.511 \pm 0.002$ | $-66.104 \pm 0.263$ |
| $E_3$ | $17.409 \pm 0.07$ | fixed at | fixed at | fixed at | $13.304 \pm 0.315$ |
| ($10^{-12}$ cm$^{-1}$) | | 11.786 | 11.786 | 11.786 | |
| $\gamma_1$ [(cm$^{-1}$)$^{-1}$] | | | $-0.135 \pm 0.002$ | $-0.2223 \pm 0.0004$ | $-0.143 \pm 0.018$ |
| $\epsilon_{\rm scale}$ (cm$^{-1}$) | | | | $51.58 \pm 0.17$ | $63.86 \pm 8.48$ |
| | | | Deduced parameters | | |
| $\epsilon_{\rm scale}$ (cm$^{-1}$) | | | $321.763 \pm 4.767$ | $51.58 \pm 0.17$ | $63.86 \pm 8.48$ |
| $c_3$ (a.u.) | $4.909 \pm 0.01$ | | | | $5.615 \pm 0.067$ |
| $c_6$ ($10^4$ a.u.) | | | | $15.14 \pm 0.05$ | $10.84 \pm 1.69$ |
| $\frac{2C_6^\Pi+C_6^\Sigma}{3}$ ($10^4$ a.u.) | | | | $3.64 \pm 0.05$ | $0.65 \pm 0.18$ |

TABLE III. The quantity $\frac{2C_6^{\Pi}+C_6^{\Sigma}}{3}$ deduced from this work and compared to values provided by [34] and [35].

| | This work | | Other works | |
|---|---|---|---|---|
| | Fit 4 | Fit 5 | Theory [34] | Expt. [35] |
| $C_6^{\Pi}$ ($10^4$ a.u.) | | | 0.8047 | 0.805 |
| $C_6^{\Sigma}$ ($10^4$ a.u.) | | | 1.205 | 1.291 |
| $\frac{2C_6^{\Pi}+C_6^{\Sigma}}{3}$ ($10^4$ a.u.) | 3.64 | 0.65 | 0.938 | 0.967 |

## V. CONCLUSION

In this paper we have shown two main results. First, the hyperfine structure existing in the $1_g$ levels, as a line splitting, can be removed (subtracted) by using a hyperfine structure calculation. Hyperfine structure in $1_g$ levels makes the analysis more complicated than usual. In order to extract the binding energies and to analyze them with a LRB-like approach, we calculate the hyperfine structure shift and subtract it. A model to calculate hyperfine structure is proposed using an intermediate basis and gives an analytical expression of the hyperfine shifts. We have checked the relevance of the model by a comparison with data.

Second, we have shown that in the case of $1_g$ levels, the term $-c_6/R^6$ can be measured from the data using a LRB-type approach. The usual LRB approach does not permit us to deduce a $c_6$ value. Including both the linear term and the second-order nonlinear terms (namely, $\gamma_{7/6}\epsilon_v^{7/6}$ and $\gamma_2\epsilon_v^2$), it is possible to extract from a fitting procedure the $c_6$ value. Even if the measurement is not very accurate, it provides an experimental value in a context where only a theoretical value has been given. The approach we have tested on $Rb_2$ $1_g$ states relies on a model [24] with some assumptions and probably could be upgraded to obtain a more accurate $c_6$ value.

## ACKNOWLEDGMENTS

The experimental work was supported by IFRAF (Institut Francilien de Recherche sur les Atomes Froids). This work was supported in part by the French Embassy in Tunis. H.J. thanks Dr. N. Reguigui and Dr. H. Abdelwahed for carefully reading the manuscript and proposing corrections.

## APPENDIX A: TABLE OF BINDING ENERGIES OF THE $1g$ LEVELS

TABLE IV. Binding energies of broad $^{87}$Rb $(5s_{1/2}+5p_{1/2})1g$ resonances. The measured binding energy $\varepsilon$ is given relative to the atomic transition $^{87}$Rb $(5S_{1/2}, F=2) \rightarrow$ $^{87}$Rb $(5P_{1/2})$ at 12 578.780 cm$^{-1}$.

| $i$ | Measured $\epsilon$ (cm$^{-1}$) | Mean $\epsilon$ (cm$^{-1}$) | Attributed $v_D-[v]$ | $N_T$ |
|---|---|---|---|---|
| 1 | 21.750(2) | 21.750(2) | not $1_g$ level | |
| 2 | 21.130(2) | 21.130(2) | 110 | 0 |
| 3 | 19.816(2) | 19.816(2) | 109 | 0 |
| 4 | 19.122(2) | 19.122(2) | not $1_g$ level | 0 |
| 5 | not detected | | 108 | |
| 6 | 17.522(2) | 17.522(2) | 107 | 0 |
| 7 | 16.538(2); 16.548(2) | 16.542(2) | 106 | 0 |
| 8 | 15.536(2); 15.538(2); 15.546(2) | | | |
| | 15.546(2); 15.596(2) | 15.552(2) | 105 | 0 |
| 9 | 14.582(2); 14.602(2); 14.604(2) | | | |
| | 14.610(2); 14.610(2) | 14.602(2) | 104 | 0 |
| 10 | 13.694(2) | 13.694(2) | 103 | 0 |
| 11 | 12.854(2); 12.862(2); 12.868(2) | 12.862(2) | 102 | 0 |
| 12 | 12.050(2); 12.054(2); 12.054(2) | | | |
| | 12.056(2); 12.062(2) | 12.056(2) | 101 | 0 |
| 13 | 11.270(2); 11.280(2); 11.300(2); 11.132(2) | 11.246(2) | 100 | 0 |
| 14 | 10.546(2); 10.562(2); 10.582(2); 10.592(2) | 10.570(2) | 99 | 0 |
| 15 | 9.870(2); 9.870(2); 9.872(2); 9.888(2) | 9.875(2) | 98 | 0 |
| 16 | 9.220(2); 9.260(2); 9.260(2); 9.275(2) | 9.254(2) | 97 | 0 |
| 17 | 8.616(2) | 8.616(2) | 96 | 0 |
| 18 | 8.034(2) | 8.034(2) | 95 | 0 |
| 19 | 7.526(2) | 7.526(2) | 94 | 0 |
| 20 | not detected | | 93 | |
| 21 | 6.570(2) | 6.570(2) | 92 | 0 |
| 22 | 6.054(2) | 6.054(2) | 91 | 0 |
| 23 | 5.676(2) | 5.672(2) | 90 | 0 |
| 24 | 5.274(2); 5.278(2) | 5.276(2) | 89 | 0 |
| 25 | 4.878(2); 4.912(2) | 4.896(2) | 88 | 0 |

TABLE V. Binding energies of the components for the 12 observed split resonances. The measured binding energy $\varepsilon$ is given relative to the atomic transition $^{87}$Rb $(5S_{1/2}, F = 2) \rightarrow$ $^{87}$Rb $(5P_{1/2})$ at 12 578.780 cm$^{-1}$.

| $i$ | $\epsilon$(cm$^{-1}$) | Attributed $v_D - [v]$ | $N_T$ | $i$ | $\epsilon$ (cm$^{-1}$) | Attributed $v_D - [v]$ | $N_T$ | $i$ | $\epsilon$ (cm$^{-1}$) | Attributed $v_D - [v]$ | $N_T$ |
|---|---|---|---|---|---|---|---|---|---|---|---|
| | | | −3 | | 3.458(2) | | −3 | | 2.540(2) | | −3 |
| | | | −2 | | 3.428(2) | | −2 | | 2.510(2) | | −2 |
| | 4.596(2) | | −1 | | −3.400(2) | | −1 | | 2.478(2) | | −1 |
| 26 | 4.562(2) | 87 | 0 | 30 | 3.372(2) | 83 | 0 | 34 | 2.452(2) | 79 | 0 |
| | 4.532(2) | | +1 | | 3.342(2) | | +1 | | 2.426(2) | | +1 |
| | 4.496(2) | | +2 | | 3.308(2) | | +2 | | 2.388(2) | | +2 |
| | 4.464(2) | | +3 | | 3.274(2) | | +3 | | 2.360(2) | | +3 |
| | | | −3 | | 3.220(2) | | −3 | | 2.360(2) | | −3 |
| | 4.296(2) | | −2 | | 3.184(2) | | −2 | | 2.322(2) | | −2 |
| | 4.266(2) | | −1 | | 3.150(2) | | −1 | | 2.298(2) | | −1 |
| 27 | 4.236(2) | 86 | 0 | 31 | 3.118(2) | 82 | 0 | 35 | 2.264(2) | 78 | 0 |
| | 4.202(2) | | +1 | | 3.082(2) | | +1 | | 2.228(2) | | +1 |
| | 4.170(2) | | +2 | | 3.044(2) | | +2 | | 2.192(2) | | +2 |
| | 4.140(2) | | +3 | | 3.008(2) | | +3 | | 2.166(2) | | +3 |
| | 4.016(2) | | −3 | | 2.972(2) | | −3 | | | | −3 |
| | 3.984(2) | | −2 | | 2.936(2) | | −2 | | | | −2 |
| | 3.956(2) | | −1 | | 2.904(2) | | −1 | | | | −1 |
| 28 | 3.928(2) | 85 | 0 | 32 | 2.864(2) | 81 | 0 | 36 | 2.102(2) | 77 | 0 |
| | 3.900(2) | | +1 | | 2.830(2) | | +1 | | 2.066(2) | | +1 |
| | 3.860(2) | | +2 | | 2.796(2) | | +2 | | 2.032(2) | | +2 |
| | 3.822(2) | | +3 | | 2.760(2) | | +3 | | 1.996(2) | | +3 |
| | 3.716(2) | | −3 | | 2.730(2) | | −3 | | | | −3 |
| | 3.688(2) | | −2 | | 2.700(2) | | −2 | | 1.950(2) | | −2 |
| | 3.656(2) | | −1 | | 2.672(2) | | −1 | | 1.912(2) | | −1 |
| 29 | 3.626(2) | 84 | 0 | 33 | 2.644(2) | 80 | 0 | 37 | | 76 | 0 |
| | 3.596(2) | | +1 | | 2.612(2) | | +1 | | 1.880(2) | | +1 |
| | 3.564(2) | | +2 | | 2.576(2) | | +2 | | 1.842(2) | | +2 |
| | 3.534(2) | | +3 | | 2.544(2) | | +3 | | 1.806(2) | | +3 |

## APPENDIX B: HYPERFINE INTERACTION IN WEAKLY BOUND MOLECULES, CALCULATED IN THE ATOMIC BASIS

We calculate the energy correction due to the hyperfine interaction (only the magnetic dipole term) in the molecule by using a perturbative method.

### 1. The intermediate basis

Because we study the asymptotic range, we use the atomic basis, namely, the linear combination of atomic orbitals (LCAO) basis. In Hund's case (c), the two $1_g$ states, associated with the projection $M = \pm 1$ of $J = 1$, can be expressed as a linear combination of atomic states labeled with $|((n_1 l_1 j_1),(n_2 l_2 j_2))J, M\rangle$, where $n_i$ denotes the principal quantum number of the atom, $l_i$ is the angular momentum, $j_i$ is the total angular momentum defined by $j_i = l_i + s_i$, with $s_i$ being the spin, and $J$ is obtained by angular composition of $j_1$ and $j_2$. With this notation, the $1_g$ states lying above the $(5s_{1/2} + 5p_{1/2})$ asymptote are expressed by

$$|1_g M = \pm 1\rangle = \frac{1}{\sqrt{2}}\{|(5s_{1/2},5p_{1/2})J = 1, M = \pm 1\rangle + |(5p_{1/2},5s_{1/2})J = 1, M = \pm 1\rangle\}. \quad \text{(B1)}$$

By taking into account the nuclear spin for each atom we introduce the noncoupled basis defined by

$$|1_g M = \pm 1\rangle |I_1 N_1\rangle |I_2 N_2\rangle, \quad \text{(B2)}$$

where $I_i = 3/2$ is the $^{87}$Rb nuclear spin and $N_i$ is its associated projection. Thus we obtain $2 \times 16$ states.

### 2. Hyperfine interaction: Magnetic dipole term

A detailed description of the hyperfine interaction in a homonuclear diatomic molecule can be found in Ref. [5]. We consider the expression of the magnetic dipole term given in Sec. 2.1$\alpha$ [36]. We denote the Hamiltonian describing the hyperfine interaction of the system of two nuclei and two electrons as $W_{hf}$. We write $W_{hf}$ as an interaction term for the nucleus denoted 1 and another one for the nucleus 2: $W_{hf} = H_{hf}(1) + H_{hf}(2)$. Each term contains the interaction between the two electrons and the nucleus and can be written as scalar products of rank 1 tensor operators, $H_{hf}(1) = W_0 \sum_{e=1,2} Q^1(1,e) I^1(1)$, with the summation being over the electrons. $I^1(1)$ is the magnetic moment of nucleus 1. $W_0$ is a constant given by $W_0 = \frac{\mu_0}{4\pi} g_S g_I \mu_B \mu_N$, where $\frac{\mu_0}{4\pi} = 10^{-7}$ SI (The International System of Units), $g_S$ and $g_I$ are the Landé factors of the electron and the nucleus, and $\mu_B$ and $\mu_N$ are the Bohr magneton and the nuclear magneton. $Q^1(1,e)$ is a tensor

operator containing the electron variables, namely, the angular momentum and the space variables, and can be expressed as $Q^1(1,e) = \frac{1}{R_{1e}^3}(L^1 - \sqrt{10}\{S^1 C^2\}^1) + \frac{8\pi}{3}\delta(R_{1e})S^1$, where $R_{1e}$ is the distance electron nucleus, $L^1$ is the angular momentum operator of the electron, $S^1$ is the electron spin, and $C^2$ is the operator associated with the harmonic spherical functions $Y_2^m$.

Using the tensor operator components, we finally get

$$W_{hf} = W_0 \sum_{e=1,2} \sum_{q=-1}^{q=1} \left[ Q_q^1(1,e) I_{-q}^1(1) + Q_q^1(2,e) I_{-q}^1(2) \right]. \tag{B3}$$

### *a. Matrix elements*

In the perturbative approach the matrix elements that we have to evaluate are then

$$W(N_1 N_2' N_1' N_2') = \langle 1_g M = \pm 1 | \langle I_1, N_1 | \langle I_2, N_2 | W_{hf} | 1_g M = \pm 1 \rangle | I_1, N_1' \rangle | I_2, N_2' \rangle,$$
$$W'(N_1 N_2 N_1' N_2') = \langle 1_g M = \pm 1 | \langle I_1, N_1 | \langle I_2, N_2 | W_{hf} | 1_g M = \mp 1 \rangle | I_1, N_1' \rangle | I_2, N_2' \rangle.$$

Using expression (B3), we deduce

$$\begin{aligned} W(N_1 N_2' N_1' N_2') = W_0 \sum_{e=1,2} \sum_q \big\{ & \langle 1_g M = \pm 1 | Q_q^1(1,e) | 1_g M = \pm 1 \rangle \delta_{N_2, N_2'} \langle N_1 | I_{-q}^1(1) | N_1' \rangle \\ & + \langle 1_g M = \pm 1 | Q_q^1(2,e) | 1_g M = \pm 1 \rangle \delta_{N_1, N_1'} \langle N_2 | I_{-q}^1(2) | N_2' \rangle \big\}, \\ W'(N_1 N_2 N_1' N_2') = W_0 \sum_{e=1,2} \sum_q \big\{ & \left\langle 1_g M = \pm 1 \right| Q_q^1(1,e) \left| 1_g M = \mp 1 \right\rangle \delta_{N_2, N_2'} \left\langle N_1 \right| I_{-q}^1(1) \left| N_1' \right\rangle \\ & + \langle 1_g M = \pm 1 | Q_q^1(2,e) | 1_g M = \mp 1 \rangle \delta_{N_1, N_1'} \langle N_2 | I_{-q}^1(2) | N_2' \rangle \big\}. \end{aligned}$$

Then by using the Wigner-Eckart theorem, the matrix elements can be expressed with $3j$ coefficients and reduced matrix elements as

$$\langle 1_g M = \pm 1 | Q_q^1(1,e) | 1_g M = \pm 1 \rangle = (-1)^{1 \mp 1} \begin{pmatrix} 1 & 1 & 1 \\ \mp 1 & q & \pm 1 \end{pmatrix} (1_g \| Q^1(1,e) \| 1_g) \tag{B4}$$

$$\langle 1_g M = \pm 1 | Q_q^1(1,e) | 1_g M = \mp 1 \rangle = (-1)^{1 \pm 1} \begin{pmatrix} 1 & 1 & 1 \\ \mp 1 & q & \mp 1 \end{pmatrix} (1_g \| Q^1(2,e) \| 1_g) \tag{B5}$$

In (B5) the $3j$ symbol is zero and implies $W'(N_1 N_2' N_1' N_2') = 0$. In (B4) the $3j$ symbol is nonzero if $q = 0$. Then, because $\langle n_1 | I_0^1(1) | n_1 \rangle = n_1$, one gets

$$W(N_1 N_2' N_1' N_2') = W_0 (-1)^{1 \mp 1} \begin{pmatrix} 1 & 1 & 1 \\ \mp 1 & 0 & \pm 1 \end{pmatrix} \sum_{e=1,2} \{ \delta_{N_2, N_2'} (1_g \| Q^1(1,e) \| 1_g) N_1 + \delta_{N_1, N_1'} (1_g \| Q^1(2,e) \| 1_g) N_2 \}.$$

Using the formula $\begin{pmatrix} j & 1 & j \\ -m & 0 & m \end{pmatrix} = (-1)^{j-m} \frac{m}{\sqrt{j(j+1)(2j+1)}}$, we finally deduce for $M = \pm 1$ states that

$$W(N_1 N_2' N_1' N_2') = \pm \frac{W_0}{\sqrt{6}} \sum_{e=1,2} \{ \delta_{N_2, N_2'} (1_g \| Q^1(1,e) \| 1_g) N_1 + \delta_{N_1, N_1'} (1_g \| Q^1(2,e) \| 1_g) N_2 \}. \tag{B6}$$

*Remark*. We point out that, in such an approach, for $0_g^-$ or $0_u^+$ states, because $J = 0,1$ and $M = 0$, we get matrix elements equal to zero because the expressions contain $\begin{pmatrix} 0 & 1 & 0 \\ 0 & 0 & 0 \end{pmatrix}$ or $\begin{pmatrix} 1 & 1 & 1 \\ 0 & 0 & 0 \end{pmatrix}$, which are null. That means that the correction due to the hyperfine interaction is zero.

### *b. Reduced matrix elements*

In expression (B6) we just have to evaluate the reduced matrix element, which is expressed by

$$(1_g\|Q^1(1,e)\|1_g) = \tfrac{1}{2}[(5s_{1/2},5p_{1/2}J=1\|Q^1(1,e)\|5s_{1/2},5p_{1/2}J=1)+(5s_{1/2},5p_{1/2}J=1\|Q^1(1,e)\|5p_{1/2},5s_{1/2}J=1)$$
$$+(5p_{1/2},5s_{1/2}J=1\|Q^1(1,e)\|5s_{1/2},5p_{1/2}J=1)+(5p_{1/2},5s_{1/2}J=1\|Q^1(1,e)\|5p_{1/2},5s_{1/2}J=1)].$$

A similar expression is obtained for nucleus 2. The calculation of $(1_g\|Q^1(1,2)\|1_g)$ will involve the distance $R_{12}$, which is on the same order of magnitude as $R$ and large compared to $R_{11}$. Thus, for a long-range molecule, $(1_g\|Q^1(1,1)\|1_g) \gg (1_g\|Q^1(1,2)\|1_g)$, and we neglect the smallest term. Then, because $Q^1(1,1)$ operates on the first electron, we deduce

$$(1_g\|Q^1(1,1)\|1_g) = \frac{(-1)^{(\frac{1}{2}+\frac{1}{2}+1+1)}3}{2}\begin{Bmatrix}1 & 1 & 1\\ \frac{1}{2} & \frac{1}{2} & \frac{1}{2}\end{Bmatrix}[(5s_{1/2}\|Q^1\|5s_{1/2})$$
$$+(5s_{1/2}\|Q^1\|5p_{1/2})+(5p_{1/2}\|Q^1\|5s_{1/2})+(5p_{1/2}\|Q^1\|5p_{1/2})],$$

with $Q^1$ being the atomic operator (one electron and one nucleus): $Q^1 = \frac{1}{r^3}(L^1 - \sqrt{10}\{S^1C^2\}^1) + \frac{8\pi}{3}\delta(r_{1e})S^1$. Selection rules due to the operator give $(5s_{1/2}\|Q^1\|5p_{1/2}) = (5p_{1/2}\|Q^1\|5p_{1/2}) = 0$. With $\{\begin{smallmatrix}1 & 1 & 1\\ \frac{1}{2} & \frac{1}{2} & \frac{1}{2}\end{smallmatrix}\} = -1/3$ one gets

$$(1_g\|Q^1(1,1)\|1_g) = (1_g\|Q^1(2,2)\|1_g) = \tfrac{1}{2}[(5s_{1/2}\|Q^1\|5s_{1/2})+(5p_{1/2}\|Q^1\|5s_{1/2})].$$

### *c. Atomic reduced matrix elements*

The elements $(5s_{1/2}\|Q^1\|5s_{1/2})$ and $(5p_{1/2}\|Q^1\|5p_{1/2})$ are one-electron reduced matrix elements which appear in the hyperfine energy calculation of the atomic hyperfine structure.

Let us consider the well-known hyperfine atomic splitting $5s_{1/2}f=1-5s_{1/2}f=2$ and $5p_{1/2}f=1-5p_{1/2}f=2$ with the respective values $\Delta^{hf}_{5s_{1/2}} = 6.834$ GHz and $\Delta^{hf}_{5p_{1/2}} = 0.816$ GHz. For an atomic state denoted $|n((lj)I)fM_f\rangle$, the hyperfine energy, calculated by a similar approach, is

$$\langle n((lj)I)fM_f|W_{hf}|n((lj)I)fM_f\rangle = W_0\frac{f(f+1)-j(j+1)-I(I+1)}{\sqrt{2j(2j+1)(2j+2)}}(nlj\|\,Q^1\,\|nlj),$$

leading to

$$\Delta^{hf}_{5s_{1/2}} = \frac{4}{\sqrt{6}}W_0(5s_{1/2}\|Q^1\|5s_{1/2}),$$
$$\Delta^{hf}_{5p_{1/2}} = \frac{4}{\sqrt{6}}W_0(5p_{1/2}\|Q^1\|5p_{1/2}),$$

and then

$$(1_g\|Q^1(1,1)\|1_g) = (1_g\|Q^1(2,2)\|1_g) = \frac{\sqrt{6}}{8W_0}\left[\Delta^{hf}_{5s_{1/2}}+\Delta^{hf}_{5p_{1/2}}\right].$$

### *d. Hyperfine energy*

Using such an approach, it is not required to calculate a radial integral, and the hyperfine energy in the large molecule is therefore related to the atomic hyperfine splitting by

$$W(N_1N_2'N_1'N_2') = \tfrac{1}{8}\left[\Delta^{hf}_{5s_{1/2}}+\Delta^{hf}_{5p_{1/2}}\right](N_1+N_2)\delta_{N_1,N_1'}\delta_{N_2,N_2'}.$$

Let us define the energy spacing $\Delta = \frac{1}{8}[\Delta^{hf}_{5s_{1/2}}+\Delta^{hf}_{5p_{1/2}}]$ and $N_T = N_1+N_2$ to get the simple expression of the energy perturbation as

$$\Delta_{hf}(N_T) = \Delta N_T.$$

### *e. Validity*

The perturbative calculation is valid as soon as $\Delta_{hf}(N_T)$ is weak compared to the binding energy of the molecule. In our approach we have also neglected terms involving $(1_g\|Q^1(1,2)\|1_g)$ and $(1_g\|Q^1(2,1)\|1_g)$, whose order of magnitude is $\sim\frac{1}{R^3}$ with $R\sim 100$ a.u. The element $(1_g\|Q^1(1,1)\|1_g)$ is evaluated by $\sim\frac{1}{r^3}$ with $r\sim 1$ a.u.

[1] A. Fioretti, D. Comparat, A. Crubellier, O. Dulieu, F. Masnou-Seeuws, and P. Pillet, Phys. Rev. Lett. **80**, 4402 (1998).

[2] C. Drag, O. Dulieu, B. Laburthe Tolra, F. Masnou-Seeuws, and P. Pillet, Phys. Rev. Lett. **86**, 2253 (2001).

[3] K. M. Jones, E. Tiesinga, P. D. Lett, and P. S. Julienne, Rev. Mod. Phys. **78**, 483 (2006).

[4] C. Amiot, Chem. Phys. Lett. **241**, 133 (1995).

[5] R. A. Cline, J. D. Miller, and D. J. Heinzen, Phys. Rev. Lett. **73**, 632 (1994).

[6] P. D. Lett, K. Helmerson, W. D. Phillips, L. P. Ratliff, S. L. Rolston, and W. E. Wagshul, Phys. Rev. Lett. **71**, 2200 (1993).

[7] M. Pichler, H. Chen, and W. C. Stwalley, J. Chem. Phys. **121**, 1796 (2004).

[8] M. Pichler, H. Chen, and W. C. Stwalley, J. Chem. Phys. **121**, 6779 (2004).

[9] R. J. LeRoy and R. B. Bernstein, J. Chem. Phys. **52**, 3869 (1970).

[10] W. C. Stwalley, Chem. Phys. Lett. **6**, 241 (1970).

[11] D. Comparat, J. Chem. Phys. **120**, 1318 (2004).

[12] H. Jelassi, B. Viaris de Lesegno, and L. Pruvost, Phys. Rev. A **73**, 032501 (2006).

[13] H. Jelassi, B. Viaris de Lesegno, and L. Pruvost, Phys. Rev. A **74**, 012510 (2006).

[14] H. Jelassi, B. Viaris de Lesegno, L. Pruvost, M. Pichler, and W. C. Stwalley, Phys. Rev. A **78**, 022503 (2008).

[15] E. R. I. Abraham, N. W. M. Ritchie, W. I. McAlexander, C. J. Williams, H. T. C. Stoof, and R. G. Hulet, J. Chem. Phys. **103**, 7773 (1995).

[16] E. R. I. Abraham, W. I. McAlexander, H. T. C. Stoof, and R. G. Hulet, Phys. Rev. A **53**, 3092 (1996).

[17] W. I. McAlexander, E. R. I. Abraham, N. W. M. Ritchie, and R. G. Hulet, Phys. Rev. A **51**, R871 (1995).

[18] V. S. Bagnato, J. Weiner, P. S. Julienne, and C. J. Williams, Laser Phys. **4**, 1062 (1994).

[19] L. P. Ratliff, M. E. Wagshul, P. D. Lett, S. L. Rolston, and W. D. Phillips, J. Chem. Phys. **101**, 2638 (1994).

[20] E. Tiesinga, K. M. Jones, P. D. Lett, U. Volz, C. J. Williams, and P. S. Julienne, Phys. Rev. A **71**, 052703 (2005).

[21] X. Wang, H. Wang, P. L. Gould, and W. C. Stwalley, Phys. Rev. A **57**, 4600 (1998).

[22] M. Kemmann, I. Mistrik, S. Nussmann, H. Helm, C. J. Williams, and P. S. Julienne, Phys. Rev. A **69**, 022715 (2004).

[23] J. D. Miller, R. A. Cline, and D. J. Heinzen, Phys. Rev. Lett. **71**, 2204 (1993).

[24] H. Jelassi, B. Viaris de Lesegno, and L. Pruvost, Phys. Rev. A **77**, 062515 (2008).

[25] L. Pruvost, D. Marescaux, O. Houde, and H. T. Duong, Opt. Commun. **166**, 199 (1999).

[26] D. Kadio, O. Houde, and L. Pruvost, Eur. Phys. Lett. **54**, 417 (2001).

[27] C. J. Williams and P. S. Julienne, J. Chem. Phys. **101**, 2634 (1994).

[28] H. Lefebvre-Brion and R. W. Field, *Perturbation in the Spectra of Diatomic Molecules* (Academic, London, 1986).

[29] We take $C_3 = 8.949(10)$ a.u., as explained in [12].

[30] We take $A = 158.39893662\ \mathrm{cm}^{-1} \equiv 7.2171865892 \times 10^{-4}$ a.u., $C_6^{\Pi} = 8.05 \times 10^3$ a.u., and $C_6^{\Sigma} = 12.91 \times 10^3$ a.u.; thus $\frac{28}{27} C_3^2/A = 11.5073 \times 10^4$ a.u. and $(2C_6^{\Pi} + C_6^{\Sigma})/3 = 0.967 \times 10^4$ [12].

[31] $(ns_{1/2} + np_{1/2})0_g^- Rb_2$ and $Cs_2$ photo-associative spectroscopy of weakly bound levels: Lu-Fano analysis coupled to an improved LeRoy-Bernstein formula; H. Jelassi, B. Viaris de Lesegno, and L. Pruvost, *Fundamental and Applied Spectroscopy: Second International Spectroscopy Conference, ISC 2007*, AIP Conf. Proc. No. 935 (AIP, New York, 2007), pp. 203–207.

[32] H. Lignier, A. Fioretti, R. Horchani, C. Drag, N. Bouloufa, M. Allegrini, O. Dulieu, L. Pruvost, P. Pillet, and D. Comparat, Phys. Chem. Chem. Phys. **13**, 18910 (2011).

[33] L. Pruvost and H. Jelassi, J. Phys. B **43**, 125301 (2010).

[34] M. Marinescu and A. Dalgarno, Phys. Rev. A **52**, 311 (1995).

[35] R. F. Gutterres, C. Amiot, A. Fioretti, C. Gabbanini, M. Mazzoni, and O. Dulieu, Phys. Rev. A **66**, 024502 (2002).

[36] M. Broyer, J. Vigué, and J. C. Lehmann, J. Phys. (France) **39**, 591 (1978).